

Search for nucleon decay using the IMB-3 detector

C. McGrew,^{1,*} R. Becker-Szendy,² C. B. Bratton,³ J. L. Breault,¹ D. R. Cady,⁴ D. Casper,⁵ S. T. Dye,² W. Gajewski,¹ K. S. Ganezer,⁶ M. Goldhaber,⁷ T. J. Haines,⁸ P. G. Halverson,¹ D. Kiełczewska,⁹ W. R. Kropp,¹ J. G. Learned,² J. M. LoSecco,⁴ S. Matsuno,² J. Matthews,¹⁰ G. McGrath,² R. Miller,⁸ L. R. Price,¹ F. Reines,¹ J. Schultz,¹ D. Sinclair,¹⁰ H. W. Sobel,¹ J. L. Stone,⁵ L. R. Sulak,⁵ R. Svoboda,¹¹ and J. C. van der Velde¹⁰

¹University of California, Irvine, California 92697-4575

²University of Hawaii at Manoa, Manoa, Hawaii 96822

³Cleveland State University, Cleveland, Ohio 44115

⁴University of Notre Dame, Notre Dame, Indiana 46556

⁵Boston University, Boston, Massachusetts 02215

⁶California State University at Dominguez Hills, Dominguez Hills, California 90747

⁷Brookhaven National Laboratory, Upton, New York 11973-5000

⁸Los Alamos National Laboratory, Los Alamos, New Mexico 87545

⁹Warsaw University, Warsaw, Poland

¹⁰University of Michigan at Ann Arbor, Ann Arbor, Michigan 48109-1120

¹¹Louisiana State University, Baton Rouge, Louisiana 70803-4001

(Received 29 May 1997; published 10 February 1999)

The IMB-3 experiment was a large water Cherenkov ring imaging detector with a fiducial mass of 3.3 kton. During a 7.6-kton-year exposure ($\sim 4.6 \times 10^{33}$ nucleon yr) 935 contained events were observed. The observed rate and characteristics are consistent with the expected backgrounds from atmospheric neutrinos. Lower limits on the nucleon lifetime are set for a wide variety of proposed decay modes. [S0556-2821(98)00323-3]

PACS number(s): 13.30.-a, 12.20.Fv, 14.20.Dh, 96.40.Tv

I. INTRODUCTION

A major goal of high energy physics is to provide a single unified explanation of the forces observed in nature. Several theories have been developed which extend the standard model to unify the electroweak and quantum chromodynamic sectors. The simplest is minimal- $SU(5)$ [1]. This theory predicts the mean proton lifetime to be $10^{29 \pm 3.2}$ yr which is ruled out by previous results [2–4]. Since minimal- $SU(5)$ was ruled out, several other models have been proposed. Perhaps the most notable are the supersymmetric models which are favored by CERN e^+e^- collider LEP results [5]. In the minimal supersymmetric model, nucleon decays via gauge bosons are strongly suppressed by the large gauge boson masses at the unification scale, leading to lifetime estimates of $10^{34.5 \pm 1.2}$ yr; however, larger decay rates are expected for Higgs mediated channels [5]. The rate of these modes is difficult to calculate, but estimates place the prediction near 10^{33} yr [6–8]. In this paper we present the final results of a search for 44 different modes of nucleon decay with the IMB-3 detector.

II. DETECTOR

The IMB-3 detector was located in the Fairport Salt Mine operated by Morton International. The detector was a large ring imaging water Cherenkov detector ~ 600 m beneath the surface and was instrumented with 2048 8-in. photomultiplier tubes. The fiducial volume contained 3.3 kton of water.

There were 935 events collected during a 851 day exposure. The detector and its calibration have been described elsewhere in detail [9,10].

The detector had a fine and coarse time scale. The fine time scale recorded a 512 ns window containing the primary interaction time. The scale had 1 ns resolution and the charge of each photomultiplier tube (PMT) hit was recorded. The coarse time scale records tube hits that occurred within 7.6 μ s after the fine scale. It was designed to detect muon decay signals and had a 15 ns resolution.

The efficiency to find a decay electron that occurred during the coarse time scale was found to be $97 \pm 5\%$ [11]. Using the detector simulation the efficiency to detect a decay electron was found to be $\sim 93\%$ [12]. Allowing for the length of the coarse window and the muon capture probability (for μ^- 's) the efficiencies to detect a muon decay are $78 \pm 4\%$ for μ^+ and $63 \pm 3\%$ for μ^- .

III. DETECTOR SIMULATION

The response of the detector was simulated in two stages. In the first stage the primary interaction was simulated and the resulting particles were tracked out of the parent nucleus. The second stage simulated the response of the IMB-3 detector to those particles.

The nucleon decay simulation includes the Fermi momentum of the nucleons. Any hadrons generated in the nucleus are then followed using a nuclear cascade model until they have left the nucleus or have decayed [13,12].

The atmospheric neutrino interaction model was developed to reproduce the neutrino interactions which occur in the detector and is used to estimate the backgrounds for the proton decay search. Several authors have calculated the

*Now at State University of New York, Stony Brook, New York 11794-3800.

flux, composition and energy distribution of atmospheric neutrinos which are generated in cosmic ray collisions occurring at the top of the atmosphere [14–18]. We have used the model of Lee and Koh [14] to predict the flux of neutrinos present at the IMB-3 detector.

The neutrino cross section on hydrogen and oxygen is calculated using the Fogli-Nardulli model, which was reformulated for use in the IMB-3 kinematic simulation [13,19,20]. It has been checked against existing neutrino data [13]. The cross section for double pion production is comparable to that of single pion production for neutrino energies above ~ 3 GeV [21,22]. It is found that double pion production accounts for 10–15% of all neutrino events above 3 GeV [13].

The statistical error in the number of events found in the IMB-3 contained event sample is smaller than the systematic error in the predicted atmospheric neutrino rate. To minimize the effects of this systematic uncertainty the atmospheric neutrino simulation is normalized to the observed event rate at $200 < E_{vis} < 1500$ GeV. This introduces a statistical error of 3.5% in the normalization which is included in the systematic error estimate. A comparison of the various neutrino flux predictions suggests that there is an uncertainty of approximately 10% in the spectral shape [14–18,12].

The background to many modes is dominated by either muon or electron neutrinos, and so the uncertainty in the ratio of ν_μ/ν_e contributes directly to the systematic error. It has been noted that there is a large discrepancy between the predicted and observed ν_μ/ν_e ratio. For limits calculated using the predicted ratio this error is taken to be 5% [14]. The ν_μ/ν_e ratio has been measured using the IMB detector to be $0.54 \pm 0.6(\text{stat})$. For limits calculated using the measured ratio this contribution to the systematic error is taken to be 10% [24,12].

The neutrino interaction model matches the kinematic data for quasi-elastic and single pion production very well. The accuracy for double pion production is difficult to determine. However, in the worst case double pion production is responsible for no more than 30% of the events in any one region. Assuming that the physics of double-pion production is not very different than expected, the systematic error should be less than 30%. The systematic errors associated with double pion production dominate those associated with single pion production, implying a systematic error of approximately 10% [13].

IV. CONTAINED EVENT SAMPLE

Two parallel analysis programs were independently developed to provide cross-checks and avoid systematic uncertainties in data reduction [11,12]. An on-line system saved all events with fewer than 900 PMT hits. Each program (designated EAST and WEST) was run on the complete data set [9]. The events found by one or both of the analysis programs were combined to form the final data sample. The sample contains 935 events collected during a 851 day exposure.

The efficiency of the combined data reduction program for atmospheric neutrino events was calculated using the de-

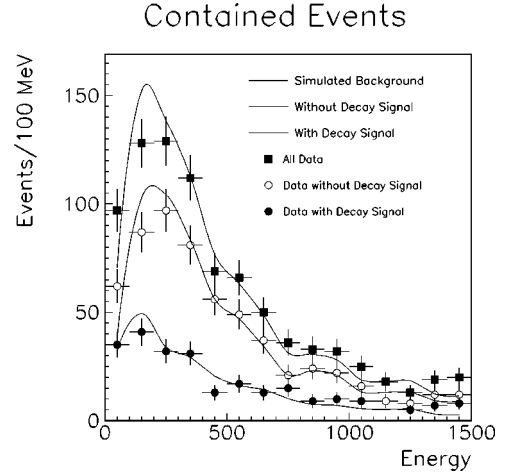


FIG. 1. The visible energy of the contained event sample and the simulated atmospheric neutrino sample. The simulation uses the measured ratio of muon type to electron type neutrinos.

tector simulation and was found to be 90% at 200 MeV, falling approximately linearly to 70% at 1 GeV. As a cross-check the combined data reduction efficiency was calculated using the assumption that the EAST and WEST analysis programs had independent efficiencies. This technique sets an upper limit on the total efficiency. This upper limit on the efficiency to save atmospheric neutrinos was found to be 95% which is consistent with the combined efficiency calculated using the simulation. Based on a comparison of the combined efficiency calculated using the detector simulation and the combined efficiency calculated using the data there is a 10% systematic uncertainty associated with the estimate of the absolute efficiency.

The visible energy of an event is proportional to the number of Cherenkov photons produced in the detector. The proportionality constant converting the number of Cherenkov photons to visible energy is chosen so that for electrons $E_{tot} \equiv E_{vis} = \kappa N_{\text{Ceren}}$. The energy resolution is $\sigma_{E_{vis}} = 2.5\%/\sqrt{E_{vis}} + 1.5\%$ where the energy is expressed in GeV. The systematic shift in the energy is less than 2% [12].

For particles other than electrons, the visible energy (i.e. total number of Cherenkov photons) as a function of total energy is calculated. This relation is non-linear for low energy particles ($E/m = \gamma < 3$); however, for higher energy particles there is a simple offset between the visible energy and total energy. For instance, the approximate energy of a muon can be calculated by adding 205 MeV to its visible energy [11,12].

The anisotropy is a convenient indicator of the net momentum in an event. Anisotropy is the magnitude of the charge weighted average from the event vertex to the PMTs. In particular, for nucleon decay into visible particles (e.g. $p \rightarrow e^+ \pi^0$) the anisotropy will be close to zero. Single particle events will have an anisotropy close to 0.7.

Figure 1 shows the visible energy and Fig. 2 shows the anisotropy of the contained events. The boxes show the distribution for all contained events. The open circles show the distribution for contained events which do not have a muon decay signal. The solid circles show the distribution for con-

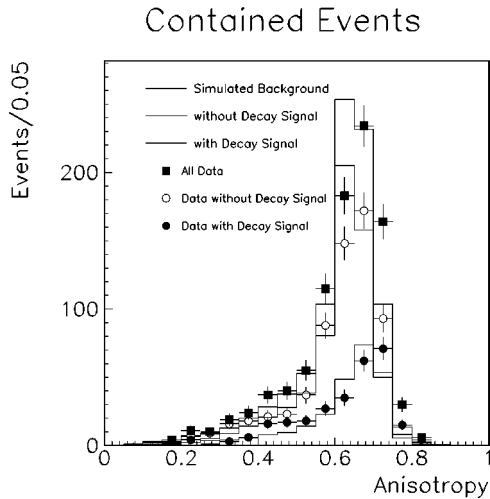


FIG. 2. The anisotropy of the contained event sample and the simulated atmospheric neutrino sample. The simulation uses the measured ratio of muon type to electron type neutrinos.

tained events with muon decay signals. The smooth lines show the predicted distribution. The ratio of electron-like to muon-like events observed in IMB-3 and Kamiokande differs from the predicted value [2,23–25]. This is accounted for by adjusting the electron-type to muon-type neutrinos used to generate the predicted distributions to the implied value.

Figures 3 and 4 show the distribution of visible energy and anisotropy. The diamonds represent events that did not have a muon decay signal. The circles represent events that had muon decay signals. The simulated distribution of visible energy for 3596 muon neutrino type and 2725 electron type neutrino events is shown in Fig. 4.

V. PHYSICS ANALYSIS

The candidate selection criteria were developed to optimize the lifetime lower limit, assuming no signal is present.

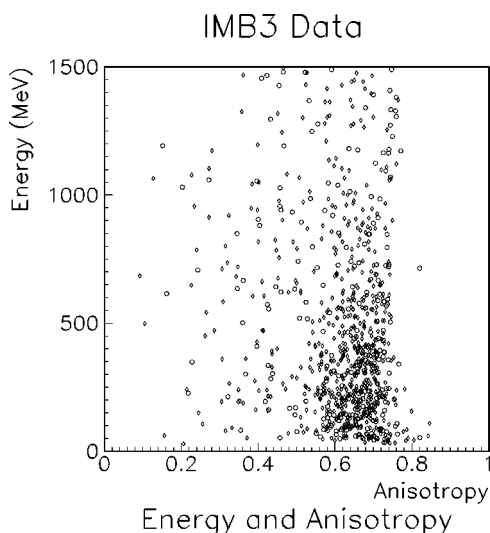


FIG. 3. The visible energy versus the anisotropy for the contained event sample. Events with muon decay signals are shown by circles. Events without muon decay signals are shown by diamonds.

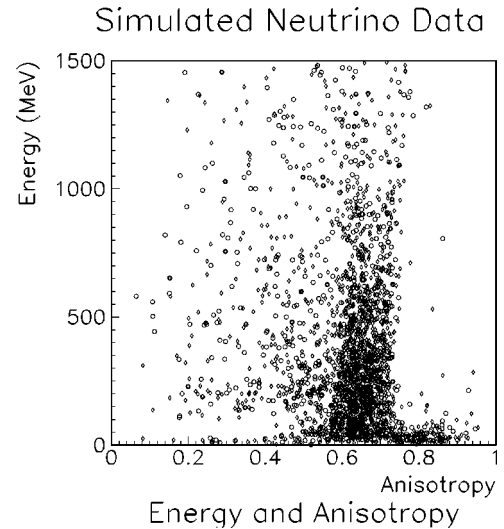


FIG. 4. The visible energy versus the anisotropy for the simulated neutrino sample. There are 2725 electron neutrino and 3596 muon neutrino events plotted. Events with muon decay signals are shown by circles. Events without muon decay signals are shown by diamonds.

For a given mode, the cuts were chosen using a sample of simulated atmospheric neutrinos and nucleon decay candidates. After the selection criteria were chosen, an independent sample of simulated neutrino and nucleon decay events was used to measure the efficiencies and backgrounds.

Each decay mode had a preliminary set of candidates selected to lie in a particular region of energy and anisotropy. Events that fell into the region were then required to have the correct number of muon decay signals.

For most modes these criteria were sufficient to reduce the background to an acceptable level; however, for certain modes which could be reconstructed particularly well, further selection criteria were applied using the number of tracks found by an automated multiple track fitter [12]. This fit is based on the ability to calculate the expected light distribution for a segment of Cherenkov track. The fit proceeded by using segments of track to construct a predicted distribution of light which was compared to the observed distribution. The fitter maximized the likelihood that the observed light came from the predicted distribution of light. For some particularly well reconstructed modes it was advantageous to do an invariant mass and unbalanced momentum analysis. This had the advantage of substantially reducing the background, at the expense of a lower efficiency.

For a few modes, it was found that a majority of the simulated background events were saved because they had been poorly fit by the multi-track fitter. The fitter was most likely to fail on events where Cherenkov rings overlapped. For these modes the events, the simulated nucleon decays and the simulated atmospheric neutrino background events were scanned to reject poor fits.

The estimated contributions to the systematic uncertainty are as follows: 3.5% from normalization statistics, 10% from the shape of the atmospheric neutrino spectrum, 10% from neutrino interaction kinematics, 10% from the absolute effi-

TABLE I. The nucleon decay lifetime limits. The cuts applied to the data are defined as follows: Cut e is an energy cut. Cut a is an anisotropy cut. Cut d is a cut on the number of muon decay signals. Cut t is a cut on the number of fitted tracks. Cut m is an invariant mass analysis. Cut s is a human scan for track verification. The limits calculated using the observed ν_μ/ν_e ratio are preferred. The limits set in this paper and those set by IMB-1 are independent and may be combined.

Mode	Cuts	Efficiency	Number of candidates	Unsubtracted limit ($\times 10^{30}$ yr)	Observed ν_μ/ν_e		Predicted ν_μ/ν_e	
					Background	Limit ($\times 10^{30}$ yr)	Background	Limit ($\times 10^{30}$ yr)
$n \rightarrow e^+ e^- \nu$	eadts	0.57	5	128	7.5	257	9.3	280
$n \rightarrow e^+ K^-$	ead	0.14	35	7	29.4	17	26.4	15
$n \rightarrow e^+ \pi^-$	eadtm	0.30	3	93	5.0	158	4.8	158
$n \rightarrow e^+ \pi^- \pi^0$	ead	0.44	38	19	34.2	52	30.6	46
$n \rightarrow e^+ \rho^-$	eadts	0.49	4	128	4.8	217	6.5	244
$n \rightarrow \mu^+ e^- \nu$	eadt	0.42	25	27	29.4	83	34.1	93
$n \rightarrow \mu^+ K^-$	ead	0.10	20	8	28.4	26	34.0	29
$n \rightarrow \mu^+ \mu^- \nu$	ead	0.81	100	15	145.0	79	188.9	138
$n \rightarrow \mu^+ \pi^-$	eadtms	0.14	1	71	1.9	90	3.7	98
$n \rightarrow \mu^+ \pi^- \pi^0$	ead	0.29	17	26	20.8	74	25.2	84
$n \rightarrow \mu^+ \rho^-$	ead	0.36	3	109	9.5	228	11.5	232
$n \rightarrow \nu \eta^0$	eadt	0.17	0	158	1.2	158	1.1	157
$n \rightarrow \nu \gamma$	ead	0.80	163	9	144.7	28	123.6	23
$n \rightarrow \nu \gamma \gamma$	eadts	0.49	5	109	7.5	219	9.3	239
$n \rightarrow \nu K^0$	ead	0.21	34	10	34.1	30	30.6	27
$n \rightarrow \nu K^{*0}$	ead	0.51	40	21	50.0	78	56.4	86
$n \rightarrow \nu \omega^0$	ead	0.28	12	33	22.5	108	26.7	114
$n \rightarrow \nu \pi^0$	eadtms	0.30	6	60	6.6	112	7.5	120
$p \rightarrow e^- \pi^+ K^+$	ead	0.46	81	13	127.2	75	160.3	111
$p \rightarrow e^+ \eta^0$	eadtm	0.28	0	315	0.2	313	0.2	314
$p \rightarrow e^+ e^+ e^-$	eadts	0.71	0	799	0.5	793	0.9	798
$p \rightarrow e^+ \gamma$	eadtm	0.60	0	675	0.1	670	0.1	673
$p \rightarrow e^+ K^0$	ead	0.12	23	11	25.2	31	26.4	32
$p \rightarrow e^+ K^{*0}$	ead	0.39	38	21	52.0	84	61.1	97
$p \rightarrow e^+ \mu^+ \mu^-$	ead	0.47	1	308	0.9	359	1.2	370
$p \rightarrow e^+ \nu \nu$	ead	0.32	152	5	153.7	17	138.7	15
$p \rightarrow e^+ \omega^0$	eadtm	0.21	7	46	10.8	107	13.5	118
$p \rightarrow e^+ \pi^0$	eadtms	0.48	0	540	0.2	540	0.2	538 ^a
$p \rightarrow e^+ \pi^0 \pi^0$	ead	0.26	2	126	0.8	147	0.7	144
$p \rightarrow e^+ \pi^+ \pi^-$	ead	0.23	16	26	23.1	82	27.2	89
$p \rightarrow \mu^- \pi^+ K^+$	ead	0.40	3	153	4.0	245	5.6	270
$p \rightarrow \mu^+ \eta^0$	eadt	0.23	3	87	2.8	126	2.8	127
$p \rightarrow \mu^+ e^+ e^-$	eadtm	0.47	0	529	1.0	529	1.1	528
$p \rightarrow \mu^+ \gamma$	eadtm	0.42	0	478	0.1	478	0.2	476
$p \rightarrow \mu^+ K^0$	eadT	0.19	4	61	7.2	120	9.5	131
$p \rightarrow \mu^+ \mu^+ \mu^-$	ead	0.60	0	675	0.3	675	0.4	673
$p \rightarrow \mu^+ \omega^0$	eadts	0.33	11	51	12.1	117	21.5	164
$p \rightarrow \mu^+ \pi^0$	eadtm	0.42	0	473	0.6	473	0.6	472
$p \rightarrow \mu^+ \pi^0 \pi^0$	ead	0.20	3	79	1.6	101	1.7	102
$p \rightarrow \mu^+ \pi^+ \pi^-$	ead	0.44	25	35	38.0	133	45.1	150
$p \rightarrow \nu K^+$	eadtm	0.41	15	50	21.4	151	29.5	182
$p \rightarrow \nu K^{*+}$	ead	0.11	7	24	9.1	51	11.3	57
$p \rightarrow \nu \pi^+$	ead	0.03	15	4	20.3	10	23.5	12
$p \rightarrow \nu \rho^+$	ead	0.54	18	56	21.7	162	25.1	179

^aCombining with IMB-1 we set a total limit of 850×10^{30} yr.

ciency, and 10% from the ν_μ/ν_e ratio. Combining the systematic errors in quadrature gives a total systematic error of $\sigma_{sys} \sim 20\%$ which is assumed to be Gaussian. This error has been included in all lifetime limits.

Using the observed ν_μ/ν_e ratio, in modes with an estimated background greater than 10 the number of candidates

is 18% below the estimated background. This is consistent with the systematic error estimate. Using the predicted ν_μ/ν_e ratio the number of candidates is 27% below the estimated background. The modes with the largest discrepancy (e.g. $p \rightarrow e^+ \pi^+ K^+$) generally have low visible energy where the observed event rate is systematically below the predicted

rate. It should be noted that many events are candidates for more than one decay mode.

The limit on the number of observed nucleon decay events for each mode has been calculated assuming the number of signal and background events are Poisson distributed and the error on the estimated background is Gaussian [26]. The probability of observing N events given a mean background of b and a mean signal of s is

$$P(N|s,b) = \frac{(s+b)^N}{N!} e^{-(s+b)} \quad (1)$$

and the probability of generating M simulated background events given an estimated mean background of \hat{b} is

$$P(M|\hat{b},c) = \frac{(\hat{b}c)^M}{M!} e^{-\hat{b}c}, \quad (2)$$

where c is the ratio of the simulated exposure to the actual exposure. The estimated background rate, \hat{b} , is different from b due to systematic error. Both b and \hat{b} have been normalized to the exposure of IMB-3. It is assumed that the probability of a particular value of \hat{b} is given by

$$P(\hat{b}|b) = \begin{cases} \frac{\frac{1}{\sigma} e^{-(b-\hat{b})^2/2\sigma^2}}{\int_0^\infty \frac{1}{\sigma} e^{-(b-\hat{b})^2/2\sigma^2} d\hat{b}} & \text{if } \hat{b} > 0, \\ 0 & \text{otherwise,} \end{cases} \quad (3)$$

where $\sigma = \sigma_{sys} b$. Combining Eqs. (2) and (3) gives

$$P(M|b,c) = \int_0^\infty P(M|\hat{b},c) P(\hat{b}|b) db. \quad (4)$$

From Eqs. (1) and (4), $P(N,M|s,b,c) = P(N|s,b)P(M|b,c)$. Applying Bayes' theorem to invert the distribution gives

$$p(s,b|N,M,c) = \frac{P(N,M|s,b,c) \pi(s) \theta(b)}{\int ds \int db P(N,M|s,b,c) \pi(s) \theta(b)} \quad (5)$$

where $\pi(s)$ and $\theta(b)$ are constant in the physical region and zero otherwise. The mean of the background is then marginalized by integrating over all possible values, $P(s|N,M,c) = \int_0^\infty P(s,b|N,M,c) db$. The 90% confidence limit is S' , such that

$$0.9 = \int_0^{S'} P(s|N,M,c). \quad (6)$$

This procedure sets a conservative upper limit on the rate of nucleon decay.

The lifetime limit for a mode m is determined by

$$\frac{\tau}{B_m} = \frac{\epsilon \mathcal{E}}{S'_m}, \quad (7)$$

where τ/B_m is the lifetime, ϵ is the candidate recovery efficiency, \mathcal{E} is the detector exposure, and S'_m is the 90% confidence limit on the mean number of nucleon decay signal events.

Table I shows the 90% confidence lower lifetime limits set by IMB-3. The lifetime limits are calculated for three different cases. The first limit is calculated without subtracting the estimated background. The second limit is calculated with the background assuming that muon to electron type neutrino ratio is the observed value. The third limit is calculated with the background assuming that ratio is the theoretically predicted value. Typically the values of the two background subtracted limits are similar.

VI. CONCLUSIONS

We have presented the final limits on nucleon decay using the IMB-3 detector. IMB-3 sees no evidence for nucleon decay in a wide variety of modes. No candidates were observed in 20% of the modes (including $p \rightarrow e^+ \pi^0$); however, in many of the modes there are substantial backgrounds and background subtraction was performed. The limits calculated using the observed ν_μ/ν_e ratio are preferred. This is the less restrictive limit in 32 of 44 limits set. In the remaining 12 cases, the limits are comparable. The limits set in this paper and those set by IMB-1 [2] are independent and may be combined.

ACKNOWLEDGMENTS

We gratefully acknowledge the support of the U.S. Department of Energy. We also thank the Morton-Thiokol Corporation which graciously housed our experiment over its ten year history. One of us (D.K.) acknowledges support by the Polish Committee for Scientific Research under grant no. 2P03B1001.

[1] H. Georgi and S. L. Glashow, Phys. Rev. Lett. **32**, 438 (1974).
 [2] T. Haines *et al.*, Phys. Rev. Lett. **57**, 1986 (1986).
 [3] R. Becker-Szendy *et al.*, Phys. Rev. D **42**, 2974 (1990).
 [4] K. S. Hirata *et al.*, Phys. Lett. B **220**, 308 (1989).
 [5] U. Amaldi *et al.*, Phys. Lett. B **281**, 374 (1992).
 [6] W. Lucha, Nucl. Phys. **B221**, 300 (1983).

[7] R. Arnowitt and P. Nath, Phys. Rev. Lett. **60**, 1817 (1988).
 [8] J. Hisano *et al.*, Nucl. Phys. **B402**, 46 (1993).
 [9] R. Becker-Szendy *et al.*, Nucl. Instrum. Methods Phys. Res. A **324**, 363 (1993).
 [10] R. Becker-Szendy *et al.*, Nucl. Instrum. Methods Phys. Res. A **326**, 1 (1994).

- [11] D. Casper, Ph.D. thesis, University of Michigan, 1990.
- [12] C. McGrew, Ph.D. thesis, University of California at Irvine, 1994.
- [13] T. Haines, Ph.D. thesis, University of California at Irvine, 1986.
- [14] H. Lee and Y. Koh, *Nuovo Cimento B* **105**, 883 (1990).
- [15] L. V. Volkova, *Sov. J. Nucl. Phys.* **31**, 784 (1980).
- [16] T. K. Gaisser *et al.*, *Phys. Rev. D* **51**, 223 (1983).
- [17] G. Barr, T. K. Gaisser, and T. Stanev, *Phys. Rev. D* **39**, 3532 (1989).
- [18] M. Honda *et al.*, “A calculation of the atmospheric neutrino flux,” technical report, ICRR, 1990.
- [19] G. L. Fogli and G. Nardulli, *Nucl. Phys.* **B160**, 116 (1979).
- [20] G. L. Fogli and G. Nardulli, *Nucl. Phys.* **B165**, 162 (1980).
- [21] S. J. Barish *et al.*, *Phys. Rev. D* **16**, 3103 (1977).
- [22] S. J. Barish *et al.*, *Phys. Rev. D* **19**, 2521 (1979).
- [23] D. Casper *et al.*, *Phys. Rev. Lett.* **66**, 2561 (1991).
- [24] R. Becker-Szendy, *Phys. Rev. D* **46**, 3720 (1992).
- [25] K. S. Hirata *et al.*, *Phys. Lett. B* **280**, 146 (1992).
- [26] T. J. Loredo, *Maximum Entropy and Bayesian Methods* (Kluwer, Amsterdam, 1990), pp. 81–142.